Prepared for submission to JCAP

arXiv:2606.05301v1 [astro-ph.CO] 3 Jun 2026

AGN Line-Intensity Mapping: A Probe of Faint Black Holes at Cosmic Noon

Eli Visbal[a] **and Greg L. Bryan**[b]

[a]Department of Physics and Astronomy and Ritter Astrophysical Research Center, University of Toledo, 2801 W. Bancroft Street, Toledo, OH, 43606, USA

[b]Department of Astronomy, Columbia University, 550 West 120th Street, New York, NY, 10027, USA

E-mail: Elijah.Visbal@utoledo.edu

Abstract. We propose line-intensity mapping (LIM) as a new probe of active galactic nuclei (AGN). By cross-correlating [Ne V] intensity maps with galaxy redshift surveys, we show that the cumulative AGN line emission can be detected even when individual sources are below the detection threshold. The 97.1 eV ionization potential of [Ne V] makes it an essentially uncontaminated tracer of AGN activity, arising from the narrow line region which is accessible even in heavily obscured AGN. We forecast signal-to-noise ratios using a Fisher matrix formalism for two hypothetical future instruments: a CDIM-like instrument targeting [Ne V] λ3426 and a PRIMA-like instrument optimized for LIM targeting [Ne V] 14.3 μm. For the CDIM-like case we find strong constraints on the product of the mean AGN intensity and bias, $S_{\rm NeV}b_{\rm NeV}$, across $z = 2$–3, with redshift-space distortions enabling individual constraints on $S_{\rm NeV}$ and $b_{\rm NeV}$. The LIM signal retains sensitivity to AGN below the 5σ direct detection threshold, which at $z = 3$ corresponds to $L_{\rm bol} \sim 5 \times 10^{43}\,{\rm erg\,s^{-1}}$ and coincides with the faint end of existing luminosity function measurements. Roughly 10% of the total signal originates from below this threshold, with the sub-threshold population detectable at $S/N = 9 - 4$ across $z = 2 - 3$ (for $S_{\rm NeV}b_{\rm NeV}$). The PRIMA-like instrument achieves slightly lower signal-to-noise but provides a complementary probe of the AGN population due to the insensitivity of the 14.3 μm line to dust attenuation. AGN LIM can potentially be applied to several scientific problems including tracing the total AGN emissivity history, constraining the black hole-halo connection at faint luminosities, and discriminating between supermassive black hole seeding mechanisms.

Contents

1 Introduction **1**

2 Methods **2**
2.1 Power Spectra 2
2.2 AGN Signal Model and Galaxy Survey 3
2.3 Noise Model 4

3 Results **5**

4 Discussion and Conclusions **8**

A Fisher Matrix Formalism **10**

1 Introduction

Line-intensity mapping (LIM) is an emerging observational technique that measures the clustering of spatial fluctuations in line emission within large-scale cosmological volumes [1, 2]. A strength of LIM is that it probes the cumulative emission from all sources in a volume, including those too faint to be detected individually. A number of LIM efforts are either planned or underway. This includes observing 21cm radiation with instruments such as *MWA*, *LOFAR*, *HERA* and *SKA* [3–6]. It also includes LIM of Lyα, Hα, CO, and [C II] with instruments like *SPHEREx* [7], *CDIM* [8], *FYST* [9], *COMAP* [10], *TIME* [11], and *CONCERTO* [12]. Up to this point, these efforts have primarily been focused on probing galaxies, reionization, or constraining cosmological parameters. In this paper, we propose LIM as a probe of active galactic nuclei (AGN). This could open a window to faint black hole populations that are difficult to observe directly.

AGN, powered by accretion onto supermassive black holes, play a fundamental role in galaxy evolution through feedback processes that regulate star formation [e.g., 13, 14], however observations of faint AGN remain challenging. For example, at $z = 3$, the AGN luminosity function (LF) reported in [15, 16] are based on data that extend down to $L_{\rm bol} \sim 3 \times 10^{43}$ erg s^{-1}. As shown below, there exists significant black hole activity in fainter AGN which can be accessed through LIM.

We focus on the [Ne V] lines, arising from Ne^{4+} ions requiring photons above 97.1 eV for their production. This ionization potential is sufficiently high that stellar populations contribute negligibly; even Wolf-Rayet stars produce few photons above the He II edge at 54.4 eV, and essentially none above 97.1 eV. This makes [Ne V] a direct tracer of AGN activity. We consider two transitions observable with hypothetical near-future facilities: the UV line at 3426 Å, accessible to a CDIM-like instrument [8], and the mid-infrared line at 14.3 μm, accessible to an instrument similar to PRIMA [17], but optimized for LIM. For each, we explore their AGN LIM capabilities at $z = 2 - 5$ below. We also note that [Ne V] emission arises from the narrow line region (NLR), which extends beyond the obscuring torus, meaning it is accessible even in heavily obscured AGN. While the UV 3426 Å line is subject to some attenuation by dust as it escapes the host galaxy, the mid-infrared 14.3 μm line is essentially unaffected by dust extinction, making it a completely unobscured probe of AGN activity.

For the instruments we consider, the [Ne V] intensity map is faint and contaminated by interloping emission lines at other redshifts. We thus consider the cross-correlation between AGN intensity maps and galaxy redshift surveys. The galaxy field provides a bright signal that improves the signal-to-noise and removes the interlopers in cross-correlation [1]. This allows the faint AGN clustering signal to be extracted even when the intensity map itself is noise-dominated. We forecast signal-to-noise ratios for both instrument concepts and demonstrate that the LIM signal carries sensitivity to AGN below the threshold where direct detections can reach. We note that cross-correlation could also be performed with other large-scale structure probes such as galaxy weak lensing or cosmic microwave background (CMB) lensing, but we defer exploring such possibilities to future work.

This paper is organized as follows. In Section 2 we describe our methods, including the theoretical framework, signal model, and noise model. In Section 3 we present our results. In Section 4 we discuss our results and present our conclusions. Throughout this work, we assume a ΛCDM cosmology with parameters consistent with [18]: $\Omega_{\rm m} = 0.32$, $\Omega_\Lambda = 0.68$, $\Omega_{\rm b} = 0.049$, $h = 0.67$, $\sigma_8 = 0.81$, and $n_{\rm s} = 0.96$.

2 Methods

2.1 Power Spectra

We consider two observables, the cross-power spectrum between a [Ne V] intensity map and a galaxy redshift survey, $P_{\rm NeV,g}$, and the galaxy auto-power spectrum $P_{\rm g}$. The [Ne V] auto-power spectrum $P_{\rm NeV}$ is in principle also measurable but is contaminated by interloping emission lines from other redshifts that are mapped to the same observed frequency (e.g., Hβ), making it unreliable as a primary observable. The cross-power spectrum mitigates this contamination since interlopers are uncorrelated with the galaxy field at the target redshift.

The power spectra are given by

$$P_{\rm NeV,g} = S_{\rm NeV}(b_{\rm NeV} + f\mu^2)(b_g + f\mu^2)P_m \tag{2.1}$$

$$P_{\rm g} = (b_g + f\mu^2)^2 P_m + \frac{1}{\bar{n}_g} \tag{2.2}$$

$$P_{\rm NeV} = S^2_{\rm NeV}(b_{\rm NeV} + f\mu^2)^2 P_m + P^{\rm shot}_{\rm NeV} + P_{\rm int} \tag{2.3}$$

where P_m is the matter power spectrum, μ is the cosine of the angle between the line of sight and the wavevector $\vec{k}$, and $f = d\ln D/d\ln a$, where D is the linear growth factor and a is the scale factor. We approximate $f \approx \Omega_m(z)^{0.55}$ following [19]. Here $\bar{n}_g$ is the mean galaxy number density, $P^{\rm shot}_{\rm NeV}$ is the AGN shot power, and $P_{\rm int}$ is the interloper power (which in principle could come from numerous lines). We have included large-scale redshift-space distortions, which are captured in the factors with μ dependency [20]. The mean intensity $S_{\rm NeV}$ and shot noise $P^{\rm shot}_{\rm NeV}$ are computed by integrating over the observed AGN luminosity function, as described below. We assume the cross-shot noise signal between the AGN and galaxy populations is negligible, this assumption is conservative in the sense that including it would add extra signal in our forecasts below. We also use the linear power spectrum, $P_{\rm m}$ throughout our calculations. Non-linear effects would primarily boost the signal on small scales, making our forecasts conservative.

The uncertainty on $P_{\rm NeV,g}$ for a single k-mode is given by

$$\sigma^2(P_{\rm NeV,g}) = \frac{P^2_{\rm NeV,g} + (P_{\rm NeV} + P_N)P_{\rm g}}{2} \tag{2.4}$$

where P_N is the instrumental noise power [1]. When computing the error in a k-bin, we account for the number of available modes N_k via an inverse variance-weighted average,

$$\frac{1}{\sigma^2_{\rm bin}(P_{\rm NeV,g})} = \sum_{\mu} \frac{N_k}{\sigma^2(P_{\rm NeV,g})} \tag{2.5}$$

where the sum is over μ-bins within the k-bin, and

$$N_k = \frac{V_{\rm surv}}{(2\pi)^3} 2\pi k^2 \Delta k \sin\theta \, \Delta\theta \tag{2.6}$$

is the number of modes in a shell of width Δk at wavenumber k and angle $\theta = \cos^{-1}\mu$, with $V_{\rm surv}$ the survey volume.

In our forecasts below, we consider two cases. In the first we conservatively neglect redshift-space distortions by setting $\mu = 0$, and compute the total signal-to-noise on the cross-power,

$$(S/N)^2 = \sum_k \frac{P^2_{\rm NeV,g}}{\sigma^2_{\rm bin}(P_{\rm NeV,g})}, \tag{2.7}$$

which corresponds to the constraint on the product $S_{\rm NeV} b_{\rm NeV}$. In the second case we include redshift-space distortions, which introduce a μ-dependent anisotropy in $P_{\rm NeV,g}$ and $P_{\rm g}$ that breaks the degeneracy between $S_{\rm NeV}$ and $b_{\rm NeV}$, allowing them to be constrained individually. We use the Fisher matrix formalism described in Appendix A to forecast the marginalized constraints on each parameter in this case. In both cases, we have assumed that cosmology is known precisely as the astrophysical uncertainties are expected to be much larger.

2.2 AGN Signal Model and Galaxy Survey

We adopt the AGN bolometric luminosity function of [15], which takes the form of a double power law, with parameters tabulated across a range of redshifts. Specifically we use the "local polished fits" given in their Table 3 and perform forecasts with the values at $z = 2$, 3, 4, and 5.

We assume that the [Ne V] λ3426 luminosity is related to the AGN bolometric luminosity via the empirical calibration of [21], who derive a relation from a sample of 94 [Ne V] λ3426-selected type 2 AGN in the COSMOS field at $z = 0.6$–1.2,

$$\log L_{\rm NeV,3426}\,[{\rm erg\,s^{-1}}] = 0.69 \log {\rm L_{bol}}\,[{\rm erg\,s^{-1}}] + 10. \tag{2.8}$$

For the [Ne V] 14.3 μm line we adopt the calibration of [22],

$$\log L_{\rm NeV,14}\,[{\rm erg\,s^{-1}}] = 0.66 \log {\rm L_{bol}}\,[{\rm erg\,s^{-1}}] + 11.25. \tag{2.9}$$

Both relations are derived from observed fluxes and therefore already account for dust extinction (though this is mainly expected to impact the λ3426 line). The mean [Ne V] intensity and shot power are then

$$S_{\rm NeV} = \int \frac{L_{\rm NeV}(L_{\rm bol})}{4\pi D_L^2} \frac{dn}{dL_{\rm bol}} \, y D_A^2 \, dL_{\rm bol}, \tag{2.10}$$

and

$$P^{\rm shot}_{\rm NeV} = \int \left(\frac{L_{\rm NeV}(L_{\rm bol})}{4\pi D_L^2}\right)^2 \frac{dn}{dL_{\rm bol}} \left(y D_A^2\right)^2 dL_{\rm bol}, \tag{2.11}$$

where D_L and D_A are the luminosity and comoving angular diameter distances respectively, and $y = d\chi/d\nu$ is the conversion factor between frequency and comoving distance.

The AGN large-scale clustering bias, $b_{\rm NeV}$, is computed via a chain of relations connecting the bolometric luminosity to the host halo mass. We note that this bias model is intended as a rough approximation to provide a reasonable fiducial model. We convert $L_{\rm bol}$ to black hole mass assuming Eddington-limited accretion,

$$M_{\rm BH} = \frac{L_{\rm bol}}{1.2 \times 10^{38}\, \lambda_{\rm Edd}}\, M_\odot \tag{2.12}$$

where we take $\lambda_{\rm Edd} = 1$. The stellar mass of the host galaxy is then estimated via $M_* = 1000\, M_{\rm BH}$ [23], and the halo mass is determined by assuming a star formation efficiency of 10%, such that $M_{\rm halo} = M_*/(0.1 \times \Omega_b/\Omega_m)$ [24]. The large-scale bias is computed from the halo mass using the fitting formula of [25], and the luminosity-weighted mean bias is given by

$$b_{\rm NeV} = \frac{\int b(L_{\rm bol})\, L_{\rm NeV}(L_{\rm bol})\, (dn/dL_{\rm bol})\, dL_{\rm bol}}{\int L_{\rm NeV}(L_{\rm bol})\, (dn/dL_{\rm bol})\, dL_{\rm bol}}. \tag{2.13}$$

We note that the exact accretion rate assumed does not strongly impact our results. Reducing the assumed Eddington fraction to $\lambda_{\rm Edd} = 0.1$ only improves our signal-to-noise at the percent level. This is because the halos which contribute to the signal are at masses where the clustering bias does not change rapidly as a function of halo mass.

As described above, we consider AGN intensity maps being cross-correlated with galaxy surveys to remove interlopers. For our forecasts presented below, we assume a galaxy survey measured directly with the CDIM-like instrument. The number density of galaxies is computed with the halo mass function from [25]. For simplicity, we assume that the star formation rate of galaxies is proportional to the halo mass with a normalization that satisfies the fit to the Madau plot [26] with

$$\mathrm{SFRD} = 0.015 \frac{(1+z)^{2.7}}{1 + [(1+z)/2.9]^{5.6}}\ \mathrm{M_\odot yr^{-1} Mpc^{-3}}. \tag{2.14}$$

We include all galaxies that are detected at 5σ confidence in the Hα line (the sensitivity of our assumed instrument is described in the next subsection). We assume the Hα luminosity is given by [27] $L_{\rm gal,H\alpha} = 1.27 \times 10^{41} (1 - f_{\rm dust}) \frac{\dot{M}_*}{\mathrm{M_\odot yr^{-1}}} \mathrm{erg\ s^{-1}}$, where $\dot{M}_*$ is the star formation rate and $f_{\rm dust} = 0.6$ is a factor accounting for dust attenuation in the galaxies [28]. We compute $b_{\rm g}$ similarly to $b_{\rm NeV}$, but without the luminosity weighting and the halo mass function instead of the AGN luminosity function (see Eq. 2.13).

2.3 Noise Model

We consider a CDIM-like instrument with a 1.2 m primary mirror, angular resolution of 2 arcsec, spectral resolution $R = 300$, and an instantaneous field of view of $8\,\mathrm{deg}^2$. This is broadly consistent with the CDIM mission concept described in [8]. We assume a survey consisting of $N_{\rm field} = 10$ independent fields each observed for a total integration time of $t = 10^8$ s, giving a total survey area of $\sim 70\,\mathrm{deg}^2$ (though we note our results are not highly sensitive to the number of fields the integration time is split across). The instrumental noise power spectrum is computed assuming photon-noise limited performance following Eq. 16 in [29].

We consider three primary interlopers for the [Ne V] λ3426 line: Hα, Hβ, and [O III] λ5007. We model Hβ line emission in the same manner as Hα for the galaxy survey described above but with the line luminosity reduced by a factor of 0.35 and the $f_{\rm dust}$ changed to 0.72. For [O III] we assume $L_{\rm gal,OIII} = 1.32 \times 10^{41}(1 - f_{\rm dust})\frac{\dot{M}_*}{\rm M_\odot yr^{-1}}{\rm erg\ s^{-1}}$, with $f_{\rm dust} = 0.7$ (these luminosities follow previous LIM calibrations [28]).

We assume that sources which are individually detected above 5σ in interloper lines are masked from the intensity map prior to computing the interloper power spectrum, removing some contamination before cross-correlation. The residual interloper power from unmasked sources is computed for each line following the geometric remapping formalism of [1], in which the interloper power spectrum is distorted due to the incorrect assumption of the target redshift. The remapped wavenumber for each line is given by

$$k' = k \int_0^{\pi/2} \sqrt{\frac{\sin^2\theta}{c_x^2} + \frac{\cos^2\theta}{c_z^2}}\, \sin\theta\, d\theta \tag{2.15}$$

where $c_x = D_A(z_{\rm int})/D_A(z_{\rm target})$ and $c_z = y(z_{\rm int})/y(z_{\rm target})$ are the ratios of the transverse and radial distance conversion factors respectively, and we have performed a spherical average over angle for simplicity.

The residual interloper power for each line is then

$$P_{\rm int}(k) = \frac{S_{\rm int}^2 b_{\rm int}^2 P_m(k') + P_{\rm shot,int}}{c_x^2 c_z}, \tag{2.16}$$

where $S_{\rm int}$ is the mean intensity of the unmasked interlopers in a particular line, $b_{\rm int}$ is their luminosity-weighted clustering bias, and $P_{\rm shot,int}$ is their shot power. We leave a full treatment of any additional interlopers for future work, but note that our approach could be conservative if the interlopers could be detected and removed using even brighter lines from the same galaxies that do not contaminate the map as interlopers.

3 Results

We begin by forecasting results for AGN LIM with the [Ne V] λ3426 line observed with our CDIM-like instrument where we have conservatively ignored redshift-space distortions by setting $\mu = 0$. In Figure 1 we present the cross-power spectrum $P_{\rm NeV,g}$ as a function of wavenumber k at $z = 3$ along with the associated 1σ error bars. We predict high signal-to-noise across a wide range of scales. We show in Figure 2 the signal-to-noise on $S_{\rm NeV} b_{\rm NeV}$ as a function of redshift for both the total signal and the contribution from AGN below the 5σ CDIM detection threshold. The total S/N is strong across $z = 2$–3 and falls toward higher redshift, driven by a combination of the declining AGN luminosity function and increased cosmological luminosity distance. For the faint-only contribution, the S/N is 9 at $z = 2$, 4 at $z = 3$, and undetectable by $z = 4$.

We note that at $z = 3$ the CDIM detection threshold for [Ne V] λ3426 corresponds to an AGN luminosity of $L_{\rm bol} \sim 5 \times 10^{43}\,{\rm erg\,s^{-1}}$. This coincides both with the faint end of the [15] observational data and thus would probe sources which are currently too faint to study. At $z = 2$ the situation is somewhat different. CDIM can detect sources only down to $L_{\rm bol} \sim 1.5 \times 10^{43}\,{\rm erg\,s^{-1}}$, while [15] have direct observational support to even lower luminosities, so the LIM measurement at $z = 2$ is probing a population that is faint but has contribution from detectable sources.

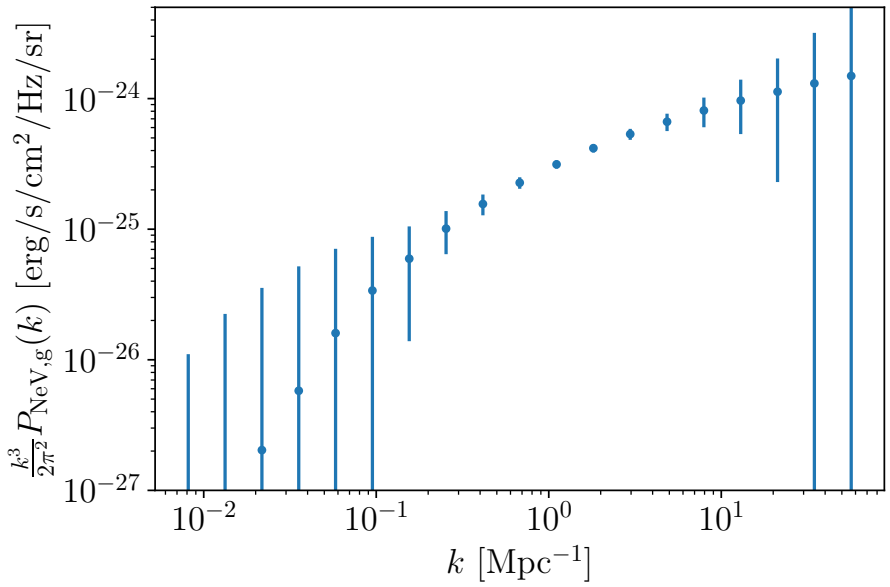


Figure 1. Cross-power spectrum at $z = 3$ for a CDIM-like survey targeting [Ne V] λ3426. Error bars show the 1σ uncertainties and data points denote central values of the assumed k-bins. Note that we conservatively do not include redshift-space distortions here, but that they are considered in the Fisher matrix calculation described in the main text.

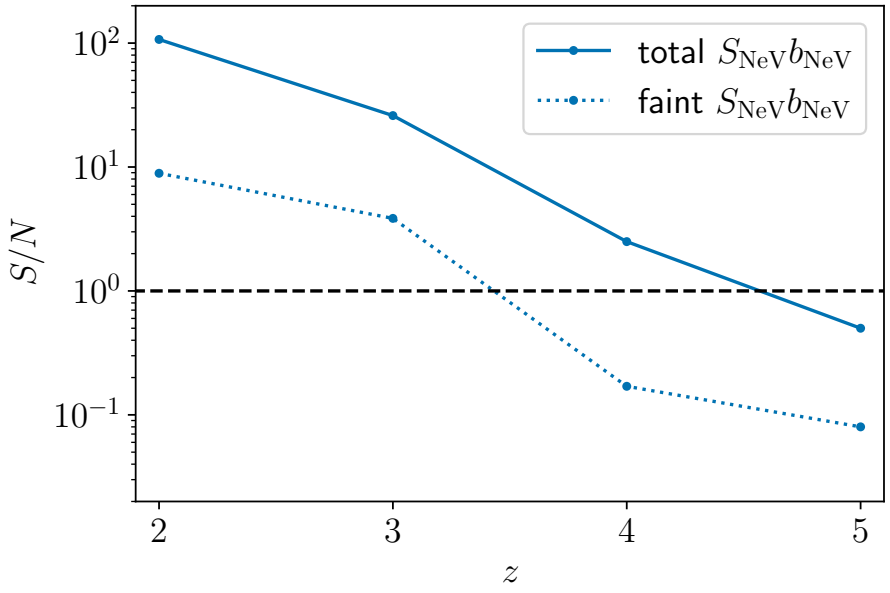


Figure 2. Signal-to-noise on $S_{\mathrm{NeV}} b_{\mathrm{NeV}}$ as a function of redshift for a CDIM-like survey cross-correlating galaxies and [Ne V] λ3426. Both the total AGN population (solid line) and the population below the CDIM 5σ direct detection limit (dotted line) are shown.

Next, we forecast how well redshift-space distortions can be utilized to break the degeneracy between the mean LIM signal and the clustering bias (see the formalism described in Appendix A). The signal-to-noise on S_{NeV} and b_{NeV} is shown in Figure 3 as a function of

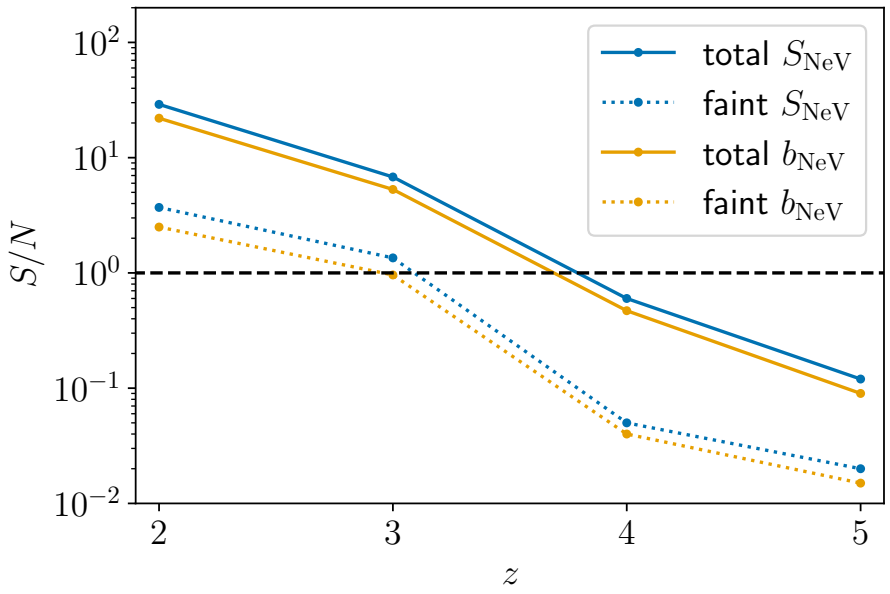


Figure 3. Signal-to-noise on $S_{\rm NeV}$ and $b_{\rm NeV}$ using redshift-space distortions as described in Appendix A, for a CDIM-like survey cross-correlating galaxies and [Ne V] λ3426. Both total (solid lines) and sub-5σ detection threshold contributions (dotted lines) are shown.

redshift, for both the total and faint-only contributions. The signal-to-noise is sufficient for meaningful individual constraints at $z = 2$–3, but not at higher redshifts.

In Figure 4 we show the cumulative fraction of the total [Ne V] mean intensity $S_{\rm NeV}$ contributed by AGN below a given bolometric luminosity. The CDIM direct detection thresholds at $z = 2$ and $z = 3$ are marked, corresponding to $L_{\rm bol} \sim 1.5 \times 10^{43}$ and $5 \times 10^{43}\,{\rm erg\,s^{-1}}$ respectively. In both cases, roughly 10% of the total signal comes from below the detection threshold. The exact fraction depends on the uncertain faint-end slope of the AGN luminosity function, and a measurement of $S_{\rm NeV}$ would therefore directly constrain the faint-end AGN emissivity in a way that is complementary to and independent of direct detection approaches. This shows that LIM is likely to inform us about the aggregate properties of faint AGN near cosmic noon.

We also forecast constraints for a hypothetical PRIMA-like instrument optimized for LIM targeting the [Ne V] 14.3 μm line, which provides a complementary extinction-free probe of the AGN population. We assume a 1.8 m primary mirror cooled to cryogenic temperatures with background-limited detectors, a spectral resolution of $R \sim 100$, and a survey consisting of $N_{\rm field} = 10$ independent fields with total integration time $t = 10^8$ s distributed across ~ 1000 spatial pixels. At $z = 3$ we forecast $S/N \sim 6$ on $S_{\rm NeV} b_{\rm NeV}$ after mitigation of the [Ne III] 15.56 μm interloper via masking of independently detected galaxies. For the faint-only contribution below $L_{\rm bol} \sim 10^{44}\,{\rm erg\,s^{-1}}$ we forecast $S/N \sim 3$. A key advantage of the 14.3 μm line over [Ne V] λ3426 is its insensitivity to dust extinction, providing an unobscured view of the AGN population that is complementary to the CDIM-like measurement. However, achieving high signal-to-noise is more challenging with our assumed instrument configuration, and the constraints are somewhat weaker than those forecasted for the CDIM-like case.

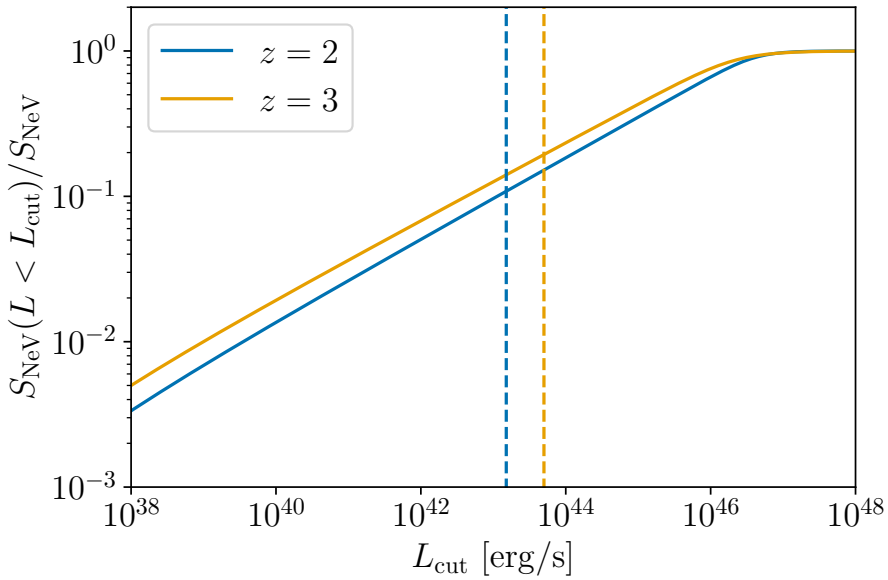


Figure 4. Cumulative fraction of the total [Ne V] mean intensity $S_{\rm NeV}$ contributed by AGN below a given bolometric luminosity, $L_{\rm cut}$, for a CDIM-like survey targeting [Ne V] λ3426. The 5σ CDIM direct detection thresholds at $z = 2$ and $z = 3$ are marked with vertical lines, both of which correspond to being above approximately 10% of the cumulative signal.

4 Discussion and Conclusions

We have proposed a line-intensity mapping technique that exploits the AGN-exclusive [Ne V] emission line to probe the faint black hole population near cosmic noon. By cross-correlating [Ne V] intensity maps with galaxy redshift surveys, we forecast constraints on the mean AGN line emissivity $S_{\rm NeV}$ and large-scale bias $b_{\rm NeV}$ for both a CDIM-like instrument targeting [Ne V] λ3426 and a hypothetical PRIMA-like instrument targeting [Ne V] 14.3 μm. We also briefly considered a *SPHEREx*-like instrument [7] targeting [Ne V] λ3426, finding $S/N \sim 1$ at $z = 2$ even with an optimistic galaxy survey. This is primarily due to its lower sensitivity, underscoring the need for a dedicated deeper survey for [Ne V] AGN LIM to be viable.

For the CDIM-like case, the total S/N on $S_{\rm NeV} b_{\rm NeV}$ is strong across $z = 2$–3 and declines at higher redshift. Redshift-space distortions enable individual constraints on $S_{\rm NeV}$ and $b_{\rm NeV}$ at $z = 2$–3, with the degeneracy becoming increasingly difficult to break at higher redshift. The key science result is the sensitivity of the LIM signal to AGN below the 5σ CDIM direct detection threshold. At $z = 3$ this threshold corresponds to $L_{\rm bol} \sim 5 \times 10^{43}\,{\rm erg\,s^{-1}}$, coinciding with the faint end of the [15] observational data, and roughly 10% of the total signal originates from below this limit. The sub-threshold population is detectable at S/N of 9 and 4 at $z = 2$ and $z = 3$ respectively, and becomes undetectable by $z = 4$. Measuring this quantity would provide an unbiased census of sources too faint to appear in any existing survey, free from the selection biases that affect stacking analyses. For the PRIMA-like case we forecast $S/N \sim 6$ on $S_{\rm NeV} b_{\rm NeV}$ and $S/N \sim 3$ on the faint population below $L_{\rm bol} \sim 10^{44}\,{\rm erg\,s^{-1}}$ at $z = 3$. While the constraints are weaker than the CDIM-like case, the 14.3 μm line would provide a dust extinction-free view of the AGN population that is complementary to the UV line measurement. In particular, the ratio of $S_{\rm NeV}$ measured in the two lines provides a direct probe of the mean dust obscuration in the host galaxy interstellar medium, averaged over the

full population including faint and obscured sources that are inaccessible to direct observation.

The choice of [Ne V] as the target line is motivated by its 97.1 eV ionization potential, which makes it an essentially uncontaminated tracer of AGN activity. Furthermore, [Ne V] emission arises from the narrow line region (NLR), which extends beyond the obscuring torus, making it accessible even in heavily obscured AGN. He II λ1640 is in principle accessible to CDIM-like instruments, however the 54.4 eV ionization potential is sufficiently low that star-forming galaxies may contribute to the mean intensity complicating the interpretation. Nevertheless, a joint measurement of He II λ1640 and [Ne V] λ3426 would be valuable. Since [Ne V] traces only AGN while He II receives contributions from both AGN and star formation, the combination probes the relative contributions of the two populations. At higher ionization potentials, coronal lines are even more AGN-exclusive but are typically expected to be fainter. Other potentially interesting lines include C IV λ1549, Mg II λ2798, [O IV] 25.89 μm, and [Ne VI] in the mid-infrared, which we leave for future investigation.

The detectability of AGN LIM opens up several scientific applications. By measuring $S_{\rm NeV}$ across multiple redshift bins one can trace the total AGN emissivity history including faint and obscured sources, providing the AGN analog of the star formation rate history [26]. Since [Ne V] traces the hard-ionizing flux above 97.1 eV, $S_{\rm NeV}$ provides a direct measurement of the evolution of the hard ionizing background near $z \sim 3$, when He II reionization is thought to occur, without requiring completeness corrections for faint or obscured sources. The bias measurement $b_{\rm NeV}$ extends the black hole-halo connection into the low luminosity regime. The combination of $S_{\rm NeV}$ and $b_{\rm NeV}$ may further constrain the AGN duty cycle and triggering mechanisms in faint sources. A joint LIM measurement of [Ne V] λ3426 and He II λ1640 would also help disentangle the three contributions to the He II intensity mapping signal from AGN, star-forming galaxies, and Population III stars, with the [Ne V] measurement providing an independent constraint on the AGN contribution that can be subtracted to isolate the remaining components. Finally, the faint-end AGN emissivity may help discriminate between supermassive black hole seeding mechanisms. For example, light seed scenarios arising from Population III stellar remnants may predict a more numerous population of faint AGN compared to massive seed scenarios even at $z{\sim}3$, leading to different predictions for $S_{\rm NeV}$.

We have demonstrated that AGN line LIM is a viable new technique for probing the faint and obscured black hole population at cosmic noon. The [Ne V] lines provide an essentially uncontaminated tracer of AGN activity accessible to near-future facilities, with the cross-correlation technique naturally suppressing interloper contamination. As next-generation instruments come online, AGN LIM may become an important new tool for understanding the demographics of the faint and obscured AGN population across cosmic time.

Acknowledgments

We thank Anne Medling, Joaquin Vieira, and Yue Shen for helpful discussions. EV acknowledges the support of NSF grant AST-2009309, NASA ATP grant 80NSSC22K0629, and STScI grant JWST-AR-05238. GLB acknowledges support from the NSF (AST-2307419), NASA TCAN award 80NSSC21K1053, and the Simons Foundation through the Learning the Universe Collaboration. The authors acknowledge the use of Claude (Anthropic) for assistance in editing portions of this manuscript.

A Fisher Matrix Formalism

We use a Fisher matrix approach to forecast constraints on the mean [Ne V] intensity $S_{\rm NeV}$ and AGN bias $b_{\rm NeV}$, with the degeneracy between these parameters broken by the anisotropic signal introduced by redshift-space distortions. For compactness we define

$$\beta_{\rm NeV} \equiv b_{\rm NeV} + f\mu^2, \quad \beta_g \equiv b_g + f\mu^2, \tag{A.1}$$

so that the power spectra may be written as

$$P_{\rm NeV,g} = S_{\rm NeV}\beta_{\rm NeV}\beta_g P_m, \quad P_{\rm g} = \beta_g^2 P_m + \frac{1}{\bar{n}_g}, \quad P_{\rm NeV} = S_{\rm NeV}^2\beta_{\rm NeV}^2 P_m + P_{\rm NeV}^{\rm shot} + P_{\rm int}. \tag{A.2}$$

The Fisher matrix is given by

$$F_{ij} = \sum_{k,\mu}\left[\frac{1}{2}{\rm Tr}\left(\mathbf{C}^{-1}\frac{\partial\mathbf{C}}{\partial\theta_i}\mathbf{C}^{-1}\frac{\partial\mathbf{C}}{\partial\theta_j}\right) + \frac{\partial\boldsymbol{\mu}^T}{\partial\theta_i}\mathbf{C}^{-1}\frac{\partial\boldsymbol{\mu}}{\partial\theta_j}\right], \tag{A.3}$$

where the sum is over k and μ bins, $\boldsymbol{\theta} = \{S_{\rm NeV}, b_{\rm NeV}, b_g\}$ is the parameter vector, and the data vector is $\boldsymbol{\mu} = (P_{\rm NeV,g}, P_{\rm g})^T$. The covariance matrix is

$$\mathbf{C} = \frac{1}{N_k}\begin{pmatrix} \frac{1}{2}(P_{\rm NeV,g}^2 + P_{\rm NeV}P_{\rm g}), & P_{\rm NeV,g}P_{\rm g} \\ P_{\rm NeV,g}P_{\rm g}, & P_{\rm g}^2 \end{pmatrix}, \tag{A.4}$$

where N_k is the number of modes in each bin. The derivatives of the mean vector with respect to each parameter are

$$\frac{\partial\boldsymbol{\mu}}{\partial S_{\rm NeV}} = \begin{pmatrix}\beta_{\rm NeV}\beta_g P_m \\ 0\end{pmatrix}, \quad \frac{\partial\boldsymbol{\mu}}{\partial b_{\rm NeV}} = \begin{pmatrix}S_{\rm NeV}\beta_g P_m \\ 0\end{pmatrix}, \quad \frac{\partial\boldsymbol{\mu}}{\partial b_g} = \begin{pmatrix}S_{\rm NeV}\beta_{\rm NeV}P_m \\ 2\beta_g P_m\end{pmatrix}. \tag{A.5}$$

The derivatives of the covariance matrix with respect to each parameter are

$$\frac{\partial\mathbf{C}}{\partial S_{\rm NeV}} = \frac{1}{N_k}\begin{pmatrix} P_{\rm NeV,g}\beta_{\rm NeV}\beta_g P_m \;+\; S_{\rm NeV}\beta_{\rm NeV}^2 P_m P_{\rm g}, & P_{\rm g}\beta_{\rm NeV}\beta_g P_m \\ P_{\rm g}\beta_{\rm NeV}\beta_g P_m, & 0 \end{pmatrix}, \tag{A.6}$$

$$\frac{\partial\mathbf{C}}{\partial b_{\rm NeV}} = \frac{1}{N_k}\begin{pmatrix} P_{\rm NeV,g}S_{\rm NeV}\beta_g P_m \;+\; S_{\rm NeV}^2\beta_{\rm NeV} P_m P_{\rm g}, & P_{\rm g}S_{\rm NeV}\beta_g P_m \\ P_{\rm g}S_{\rm NeV}\beta_g P_m, & 0 \end{pmatrix}, \tag{A.7}$$

$$\frac{\partial\mathbf{C}}{\partial b_g} = \frac{1}{N_k}\begin{pmatrix} P_{\rm NeV,g}S_{\rm NeV}\beta_{\rm NeV}P_m \;+\; P_{\rm NeV}\beta_g P_m, & S_{\rm NeV}\beta_{\rm NeV}P_m P_{\rm g} \;+\; 2P_{\rm NeV,g}\beta_g P_m \\ S_{\rm NeV}\beta_{\rm NeV}P_m P_{\rm g} \;+\; 2P_{\rm NeV,g}\beta_g P_m, & 4P_{\rm g}\beta_g P_m \end{pmatrix}. \tag{A.8}$$

Marginalized constraints on individual parameters are obtained from the diagonal of the inverse Fisher matrix, $\sigma(\theta_i) = (F^{-1})_{ii}^{1/2}$.

References

[1] E. Visbal and A. Loeb, *Measuring the 3D clustering of undetected galaxies through cross correlation of their cumulative flux fluctuations from multiple spectral lines*, *JCAP* **2010** (2010) 016 [1008.3178].

[2] T.-C. Chang and A. Lidz, *Line-Intensity Mapping*, *arXiv e-prints* (2026) arXiv:2602.03011 [2602.03011].

[3] Jeli´c, V., de Bruyn, A. G., Mevius, M., Abdalla, F. B., Asad, K. M. B., Bernardi, G. et al., *Initial lofar observations of epoch of reionization windows - ii. diffuse polarized emission in the elais-n1 field*, *A&A* **568** (2014) A101.

[4] D.R. DeBoer, A.R. Parsons, J.E. Aguirre, P. Alexander, Z.S. Ali, A.P. Beardsley et al., *Hydrogen epoch of reionization array (HERA)*, *Publications of the Astronomical Society of the Pacific* **129** (2017) 045001.

[5] L. Koopmans, J. Pritchard, G. Mellema, J. Aguirre, K. Ahn, R. Barkana et al., *The cosmic dawn and epoch of reionisation with ska*, p. 001, 05, 2015, DOI.

[6] N. Barry, G. Bernardi, B. Greig, N. Kern and F. Mertens, *SKA-low intensity mapping pathfinder updates: deeper 21 cm power spectrum limits from improved analysis frameworks*, *Journal of Astronomical Telescopes, Instruments, and Systems* **8** (2022) 011007 [2110.06173].

[7] O. Doré, J. Bock, M. Ashby, P. Capak, A. Cooray, R. de Putter et al., *Cosmology with the SPHEREX All-Sky Spectral Survey*, *arXiv e-prints* (2014) arXiv:1412.4872 [1412.4872].

[8] A. Cooray, T.-C. Chang, S. Unwin, M. Zemcov, A. Coffey, P. Morrissey et al., *Cosmic Dawn Intensity Mapper*, in *Bulletin of the American Astronomical Society*, vol. 51, p. 23, Sept., 2019 [1903.03144].

[9] C. Karoumpis, B. Magnelli, E. Romano-Díaz, M. Haslbauer and F. Bertoldi, *[CII] line intensity mapping the epoch of reionization with the Prime-Cam on FYST. I. Line intensity mapping predictions using the Illustris TNG hydrodynamical simulation*, *A & A* **659** (2022) A12 [2111.12847].

[10] K.A. Cleary, J. Borowska, P.C. Breysse, M. Catha, D.T. Chung, S.E. Church et al., *COMAP Early Science. I. Overview*, *ApJ* **933** (2022) 182 [2111.05927].

[11] G. Sun, T.C. Chang, B.D. Uzgil, J.J. Bock, C.M. Bradford, V. Butler et al., *Probing Cosmic Reionization and Molecular Gas Growth with TIME*, *ApJ* **915** (2021) 33 [2012.09160].

[12] CONCERTO Collaboration, P. Ade, M. Aravena, E. Barria, A. Beelen, A. Benoit et al., *A wide field-of-view low-resolution spectrometer at APEX: Instrument design and scientific forecast*, *A & A* **642** (2020) A60 [2007.14246].

[13] J. Silk and M.J. Rees, *Quasars and galaxy formation*, *A & A* **331** (1998) L1 [astro-ph/9801013].

[14] D.J. Croton, V. Springel, S.D.M. White, G. De Lucia, C.S. Frenk, L. Gao et al., *The many lives of active galactic nuclei: cooling flows, black holes and the luminosities and colours of galaxies*, *MNRAS* **365** (2006) 11 [astro-ph/0508046].

[15] X. Shen, P.F. Hopkins, C.-A. Faucher-Giguère, D.M. Alexander, G.T. Richards, N.P. Ross et al., *The bolometric quasar luminosity function at $z = 0$-7*, *MNRAS* **495** (2020) 3252 [2001.02696].

[16] E. Pouliasis, A. Ruiz, I. Georgantopoulos, F. Vito, R. Gilli, C. Vignali et al., *Active galactic nucleus X-ray luminosity function and absorption function in the Early Universe ($3 \leq z \leq 6$)*, *A & A* **685** (2024) A97 [2401.13515].

[17] J. Glenn, M. Meixner, C.M. Bradford, K. Pontoppidan, A. Pope, T. Kataria et al., *PRIMA mission concept*, *Journal of Astronomical Telescopes, Instruments, and Systems* **11** (2025) 031628.

[18] Planck Collaboration, N. Aghanim, Y. Akrami, M. Ashdown, J. Aumont, C. Baccigalupi et al., *Planck 2018 results. VI. Cosmological parameters*, *A & A* **641** (2020) A6 [1807.06209].

[19] E.V. Linder, *Cosmic growth history and expansion history*, *Phys Rev D* **72** (2005) 043529 [astro-ph/0507263].

[20] N. Kaiser, *Clustering in real space and in redshift space*, *MNRAS* **227** (1987) 1.

[21] L. Barchiesi, C. Vignali, F. Pozzi, R. Gilli, M. Mignoli, C. Gruppioni et al., *COSMOS2020: Investigating the AGN-obscured accretion phase at $z \sim 1$ via [Ne V] selection*, *A & A* **685** (2024) A141 [2403.03251].

[22] C. Gruppioni, S. Berta, L. Spinoglio, M. Pereira-Santaella, F. Pozzi, P. Andreani et al., *Tracing black hole accretion with SED decomposition and IR lines: from local galaxies to the high-z Universe*, *MNRAS* **458** (2016) 4297 [1603.02818].

[23] J. Kormendy and L.C. Ho, *Coevolution (or not) of supermassive black holes and host galaxies*, *ARA&A* **51** (2013) 511.

[24] P.S. Behroozi, R.H. Wechsler and C. Conroy, *The average star formation histories of galaxies in dark matter halos from $z = 0$–8*, *ApJ* **770** (2013) 57.

[25] R.K. Sheth, H.J. Mo and G. Tormen, *Ellipsoidal collapse and an improved model for the number and spatial distribution of dark matter haloes*, *MNRAS* **323** (2001) 1 [astro-ph/9907024].

[26] P. Madau and M. Dickinson, *Cosmic Star-Formation History*, *ARA&A* **52** (2014) 415 [1403.0007].

[27] R.C. Kennicutt, Jr., *Star Formation in Galaxies Along the Hubble Sequence*, *ARA&A* **36** (1998) 189 [astro-ph/9807187].

[28] Y. Gong, A. Cooray, M.B. Silva, M. Zemcov, C. Feng, M.G. Santos et al., *Intensity Mapping of Hα, Hβ, [OII], and [OIII] Lines at $z < 5$*, *ApJ* **835** (2017) 273 [1610.09060].

[29] P. Comaschi, B. Yue and A. Ferrara, *Observational challenges in Lyα intensity mapping*, *MNRAS* **463** (2016) 3193 [1605.05733].